LANGMUIR Article
Cite This: Langmuir 2018, 34, 8245−8254
pubs.acs.org/Langmuir

Probing Additive Loading in the Lamellar Phase of a Nonionic Surfactant: Gibbs Ensemble Monte Carlo Simulations Using the SDK Force Field

Mona S. Minkara,[†] Rebecca K. Lindsey,[†] Robert H. Hembree,[†] Connor L. Venteicher,[†] Sumanth N. Jamadagni,[‡] David M. Eike,[‡] Ahmad F. Ghobadi,[‡] Peter H. Koenig,[‡] and J. Ilja Siepmann*[,†,§]

[†]Department of Chemistry and Chemical Theory Center, University of Minnesota, 207 Pleasant Street SE, Minneapolis, Minnesota 55455, United States

[‡]Computational Chemistry, Modeling and Simulation, The Procter & Gamble Company, 8256 Union Centre Blvd, West Chester, Ohio 45069, United States

[§]Department of Chemical Engineering and Materials Science, University of Minnesota, 421 Washington Avenue SE, Minneapolis, Minnesota 55455, United States

Supporting Information

ABSTRACT: Understanding solute uptake into soft microstructured materials, such as bilayers and worm-like and spherical micelles, is of interest in the pharmaceutical, agricultural, and personal care industries. To obtain molecular-level insight on the effects of solutes loading into a lamellar phase, we utilize the Shinoda−Devane−Klein (SDK) coarse-grained force field in conjunction with configurational-bias Monte Carlo simulations in the osmotic Gibbs ensemble. The lamellar phase is comprised of a bilayer formed by triethylene glycol mono-*n*-decyl ether (C10E3) surfactants surrounded by water with a 50:50 surfactant/water weight ratio. We study both the unary adsorption isotherm and the effects on bilayer structure and stability caused by *n*-nonane, 1-hexanol, and ethyl butyrate at several different reduced reservoir pressures. The nonpolar *n*-nonane molecules load near the center of the bilayer. In contrast, the polar 1-hexanol and ethyl butyrate molecules both load with their polar bead close to the surfactant head groups. Near the center of the bilayer, none of the solute molecules exhibits a significant orientational preference. Solute molecules adsorbed near the polar groups of the surfactant chains show a preference for orientations perpendicular to the interface, and this alignment with the long axis of the surfactant molecules is most pronounced for 1-hexanol. Loading of *n*-nonane leads to an increase of the bilayer thickness, but does not affect the surface area per surfactant. Loading of polar additives leads to both lateral and transverse swelling. The reduced Henry's law constants of adsorption (expressed as a molar ratio of additive to surfactant per reduced pressure) are 0.23, 1.4, and 14 for *n*-nonane, 1-hexanol, and ethyl butyrate, respectively, and it appears that the SDK force field significantly overestimates the ethyl butyrate−surfactant interactions.

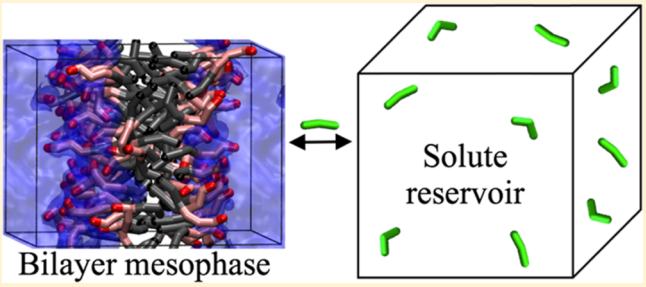

INTRODUCTION

Knowledge of the uptake of solutes into microstructured soft materials can be used across many fields to improve material performance. In the pharmaceutical industry, transport of hydrophobic compounds, such as Ibuprofen,[1] through hydrophilic media, such as human blood, can be optimized by adjusting the micellar structure of the surfactant drug delivery vehicle.[2−4] Furthermore, studying the uptake of solutes into bilayer systems, like the stratum corneum, the outermost layer of human skin, can improve micellar design for drug delivery through such systems.[5] In industries like agriculture, manipulating solute uptake in micellar systems prevents irreversible denaturation and loss of biological activity,[6] which is important for the delivery of pesticides to plants and for the extraction of oil and protein from crops. Formulations with micellar mesophases are also utilized to enhance the loading capacity for fragrance compounds and other additives in personal care or cleaning products[7,8] and to apply hydrophobic coatings over clothing and windshields.[9]

Because of several competitive and cooperative effects, surfactant systems are extremely complex. Solubility, polarity, and shape/rigidity of the solute influence their uptake.

Received: March 2, 2018
Revised: June 11, 2018
Published: June 14, 2018

DOI: 10.1021/acs.langmuir.8b00687
Langmuir 2018, 34, 8245−8254

Table 1. Molecules and SDK Bead Types

molecule	SDK formula	bead type	chemical formula	molar mass (g/mol)
C10E3	CT−CM−CM−EO−EO−EO−OA	CT	$CH_3-CH_2-CH_2-$	43.1
n-nonane	CT−CM−CT	CM	$-CH_2-CH_2-CH_2-$	42.1
1-hexanol	CT2−CM−OA	EO	$-CH_2-O-CH_2-$	44.1
ethyl butyrate	CT2−EST1−CT2	OA	$HO-CH_2-$	31.0
water trimer	W	CT2	CH_3-CH_2-	29.1
		EST1	$-CH_2-CO-O-$	58.0
		W	$[H_2O]_3$	54.0

Furthermore, aggregates, mesophases, and the physical properties of the solution modify the extent to which favorable solute sorption domains exist.[10,11] These properties can influence the structure of microstructured soft materials, the loading of solutes, and, in conjunction, these properties can modify solute uptake. Because of competitive effects, water penetration into micellar and bilayer structures can result in decreased loading of polar solutes.[10,12,13]

Despite a host of experimental studies on surfactant systems,[14−21] it is difficult to determine structural properties of the system on a molecular level. Spectroscopy and scattering methods are limited to the structural information related to the mesophase, head-group area, and bilayer repeat distance. Many of the finer details are left to be extracted through models containing a large number of assumptions that are difficult to test experimentally. For example, the structure of water in the vicinity of ether groups like those found in C*x*E*y* surfactants, such as triethylene glycol mono-*n*-decyl ether (C10E3), has been probed by vibrational spectroscopy,[22,23] scattering,[24] nuclear magnetic resonance,[25,26] and thermodynamic models.[27] However, important questions concerning solute uptake into micellar aggregates and soft microstructured materials remain even after such studies: How does varying the solute's chemical potential affect its loading into a surfactant bilayer? How does the uptake of different solutes affect bilayer structure and stability? What is the orientation and location of solutes loaded into the bilayer?

Molecular simulation provides an alternative approach for investigating the microscopic structure of complex chemical systems. Many studies have been conducted for these systems through simulation;[28−36] however, the majority rely on molecular dynamics of closed systems, which are limited to prespecified system compositions. Use of a closed system comes with severe limitations: either simulating the system in the infinite dilution regime (i.e., only a single solute molecule is present in the system) or simulating a system with a finite number of solute molecules, but without controlling concentration in different mesophase regions. Continuum-solvation methods are available that can quickly predict the amount of a solute that can load into soft microstructured materials.[37] However, information about the structural orientation and positioning of the solutes at the molecular level is not obtainable with continuum methods. The other option is to examine structured surfactant materials using open system approaches, such as grand canonical Monte Carlo; however, the prior applications were primarily focused on coalescence of surfactant-coated droplets[38] or prediction of the critical micelle concentration,[35] or the model was highly simplified.[34]

In this study, we study uptake in a nonionic surfactant bilayer through molecular simulation using the osmotic Gibbs ensemble Monte Carlo approach.[39] In our simulations, the water−surfactant mesophase is contained in one simulation box and is in thermodynamic contact with a second box containing a vapor phase of the solute of interest, where only the solute can transfer between simulation boxes. By varying the reduced pressure (or chemical potential) of the solute molecules in the reservoir and allowing for fluctuations in lateral and transverse dimensions of the mesophase box, we can predict solute loading and investigate the resulting structural changes in the bilayer. From this, we can shed light on how bilayer structure and solute uptake are interrelated. Loading of *n*-nonane, 1-hexanol, and ethyl butyrate in a lamellar C10E3 system using the coarse-grained Shinoda−Devane−Klein (SDK) force field[40,41] is investigated with the goals of establishing simulation protocols and understanding how solute functionality influences loading and structural changes. The SDK force field offers significant computational speedup compared to united-atom or all-atom force fields because it reduces the number of interaction sites by a factor of 3−7 for C10E3 and of 9−12 for water and does not include long-range electrostatic interactions.

COMPUTATIONAL METHODS

Before simulating the loading of the surfactant bilayer, various support calculations must be performed to establish appropriate system properties. The saturated vapor pressure of each solute of interest (*n*-nonane, 1-hexanol, or ethyl butyrate) is calculated at a temperature of 300 K using a two-box isochoric−isothermal Gibbs ensemble.[39,42] In addition, a PACKMOL[43]-initialized C10E3 bilayer in water (50:50 weight percent) is equilibrated in a modified constant-stress ensemble (where changes in surface area and transverse thickness are allowed)[44,45] at a pressure of 1 atm and a temperature of 300 K. Given these supporting simulations, loading of each solute of interest into the equilibrated bilayer is performed. All simulations have been completed using the MCCCS-MN (Monte Carlo for complex systems-Minnesota) software suite.[46]

The SDK force field is used to model the molecules in a coarse-grained fashion throughout the simulations.[40,41,47] Bead types for molecules considered in this study are listed in Table 1 (and force field parameters are provided in the Supporting Information (SI) Tables S1−S3). As is required by the SDK force field, a 15 Å cutoff without tail corrections is used here for all simulations.

To compute the saturated vapor pressure of each solute of interest, a two-box system composed of 500 molecules in the *NVT* Gibbs ensemble[39,42] is used. In both phases, the solute molecules can translate, rotate, and undergo conformational changes using configurational-bias Monte Carlo (CBMC) moves.[48,49] To reach thermodynamic equilibrium, volume exchange moves between both simulation boxes are carried out with frequency and maximum displacements adjusted to yield on average one accepted move per Monte Carlo (MC) cycle (1 MC cycle = *N* moves, where *N* is the total number of molecules in the system). CBMC approaches are used to aid molecular transfers[50] with frequency, and CBMC parameters are adjusted to yield on average one accepted move per 10 MC cycles. The remaining moves are divided equally amongst CBMC conformational, translational, and rotational moves in a manner commensurate

DOI: 10.1021/acs.langmuir.8b00687
Langmuir 2018, 34, 8245−8254

with the respective number of degrees of freedom. The simulations are run for 500 000 MC cycles across 16 independent simulations to yield a saturated vapor pressure with a relative standard error of the mean that is less than 0.5%, and the results are presented in Table 2.

Table 2. Saturated Vapor Pressures and Compressibility Factors at T = 300 K

solute	p_{sat}^{SDK} (kPa)	z	p_{sat}^{exp} (kPa)	references
n-nonane	0.609_3	1.001_1	0.603	51
1-hexanol	3.04_1	0.9978_3	0.136	52
ethyl butyrate	4.43_2	0.9958_2	2.55	53

The SDK force field yields a vapor pressure for *n*-nonane in excellent agreement with experiment, but those for ethyl butyrate and 1-hexanol are overpredicted by factors of 1.7 and 22, respectively. This is likely driven by SDK parameters being fit to condensed phase properties, such as hydration free energy and liquid/liquid surface tensions rather than saturated vapor pressures.[41]

The water−surfactant mesophase system, corresponding to a 50/50 weight percent ratio, consists of 100 C10E3 molecules and 538 water beads, where each bead represents three water molecules in the SDK force field, and is initialized by packing water and C10E3 molecules into one simulation box via PACKMOL.[43] The surfactants are roughly oriented toward their eventual bilayer form (50 C10E3 molecules in each leaflet) and initialized with a head-group area like that in experiment.[18]

To gather unary loading isotherms for the solute surfactant−water mixture, six independent production simulations for *n*-nonane and 1-hexanol and eight for ethyl butyrate, in the $N_{WAT}N_{CE}N_{SOL}p_{SOL}p_{meso}T$ osmotic constant-stress Gibbs ensemble,[39,42] are run at T = 300 K, where the subscripts "WAT", "CE", "SOL", and "meso" refer to water, C10E3, solute, and surfactant mesophase, respectively. These simulations differ by the external pressure applied to the vapor phase, set to 2, 4, 8, 16, 32, and 64% of the calculated saturated vapor pressure (p_{sat}) with the addition of 0.5 and 1% of the calculated saturated vapor pressure for ethyl butyrate. In each simulation, two boxes in thermodynamic contact are set up. The first box contains the bilayer at p_{meso} = 1 atm. The second box contains an ideal gas of either *n*-nonane, 1-hexanol, or ethyl butyrate (i.e., intermolecular interactions are turned off as justified by the compressibility factor of the saturated vapor phase being very close to unity for all three solutes, see Table 2). The pressure of this solute reservoir box, p_{sol}, is set to a given fraction of the calculated saturated vapor pressure. Molecules in both boxes can translate, and with the exception of water, rotate, and undergo conformational changes. The volume of each box is allowed to vary independently, with an accepted volume move once every MC cycle, on average. For the box containing the surfactant bilayer, the volume move is either a change in either the lateral area (i.e., coupled change in the x- and y-dimensions) or the thickness in the z-dimension with the corresponding scaled displacements in the center-of-mass coordinates of all molecules. A solute particle transfer move between the two boxes is accepted on average once every 10 MC cycles to ensure sufficient time for relaxation of the mesophase structure. The remaining moves are divided equally amongst CBMC conformational, translational, and rotational moves.

The simulations were run for at least 2 000 000 MC cycles, with at least 1 000 000 MC cycles for equilibration and 1 000 000 MC cycles for production. We used one simulation for equilibration and twelve independent simulations for production that were averaged together for analysis. The evolution of the solute loadings during equilibration (starting with no solute molecules in the mesophase) and production is illustrated in Figure S1 in the SI. The soft mesophases investigated in this study pose sampling challenges for molecular simulations. On the one hand, larger-scale structural fluctuations of the lamellar system are better sampled through collective motion of multiple molecules; on the other hand, the low concentration of additives and spatially disconnected regions of low free energy for additives requires special moves to sample their spatial distribution beyond slow mass transport through diffusive motion. With the system sizes investigated here, we would like to argue that MC simulations are adequate to sample collective structure rearrangements, but essential to sample additive distribution. For larger system sizes and complex surfactant mixtures, hybrid molecular dynamics/MC schemes would likely be most advantageous.

RESULTS AND DISCUSSION

Adsorption Isotherms. Analysis of the loading behavior is needed to understand how different solutes distribute into a surfactant bilayer and how the loading of each unique solute type affects the structure of the bilayer. We find that uptake of the *n*-nonane, 1-hexanol, and ethyl butyrate molecules differs significantly (see Figure 1). On average, 1-hexanol loads at amounts roughly 6 times greater than *n*-nonane, whereas ethyl butyrate loads at amounts roughly 20 times greater than *n*-nonane.

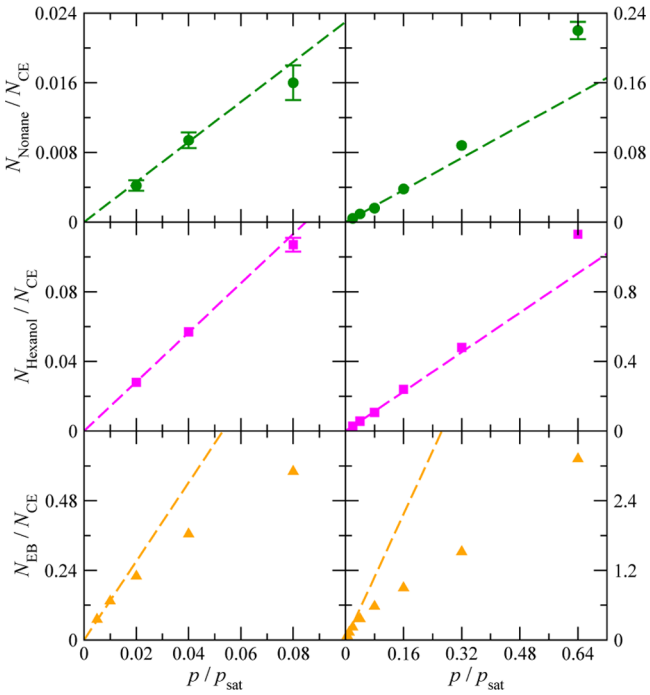

Figure 1. Loading of *n*-nonane (top), 1-hexanol (middle), and ethyl butyrate (bottom) versus the reduced pressure of the solute. The green circles, magenta squares, and orange triangles represent the loading determined from simulation, while the dashed lines represent Henry's law fit. The left column shows a zoom-in of the low reduced pressure region, while the right column shows the complete range.

Henry's law can be expressed by eq 1, which relates the loading of the solute in terms of the average number of solute molecules adsorbed, N_{solute}, per number of surfactant molecules, N_{CE} (or, analogously, as mass of solute per mass of surfactant), to its reduced pressure, p/p_{sat}, via Henry's law constant, K_H.

$$\frac{N_{solute}}{N_{CE}} = K_H\left(\frac{p}{p_{sat}}\right) \quad (1)$$

One may define the loading of the solutes also in terms of mole fraction (as shown in Figure S2 in the SI), yielding the following relationship

DOI: 10.1021/acs.langmuir.8b00687
Langmuir 2018, 34, 8245−8254

$$\frac{N_{\text{solute}}}{N_{\text{CE}} + N_{\text{solute}}} = K_{\text{H}}\left(\frac{p}{p_{\text{sat}}}\right) \tag{2}$$

It should be noted that water is not included here in the calculation of mole fraction because the number of water molecules is 16 times larger than N_{CE} (because $N_{\text{solute}} \ll 3N_{\text{WAT}} + N_{\text{CE}}$, the denominator in eq 2 would be nearly constant and yield the same behavior as eq 1). To obtain more information on which definition is more suitable for our system of solutes adsorbing into a liquid bilayer, we plotted the Gibbs free energy of transfer as a function of reduced pressure (see Figure 2). The Gibbs free energy of transfer can be expressed by eq 3

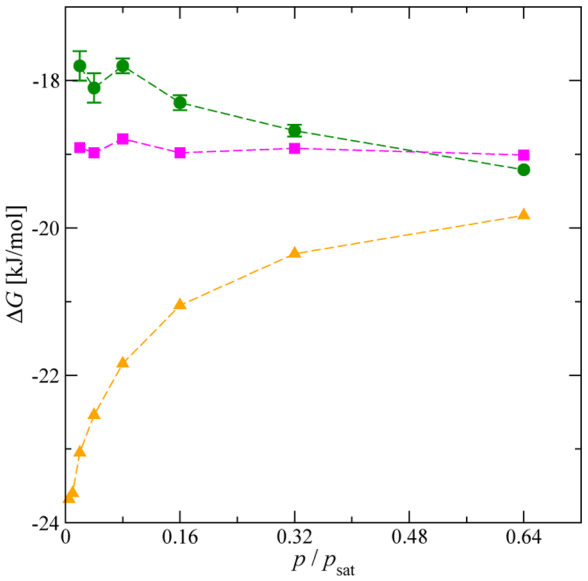

Figure 2. Gibbs free energy of transfer versus reduced pressure. The green circles, magenta squares, and orange triangles represent data for *n*-nonane, 1-hexanol, and ethyl butyrate, respectively. The dashed lines are drawn for clarity.

$$\Delta G = -RT \ln K = -RT \ln \frac{\rho_{\text{LIQ}}}{\rho_{\text{VAP}}} \tag{3}$$

where R is the gas constant, T is the absolute temperature, K is the equilibrium constant, and ρ_{LIQ} and ρ_{VAP} are the number densities of solute in the mesophase and in the vapor reservoir, respectively. We observe that K_{H} defined as a solute/surfactant molar ratio (see eq 1, Figure 1) more closely follows the trends of the transfer free energy than K_{H} defined in terms of mole fraction (see eq 2, Figure S2). The former is therefore more representative of the thermodynamics for these systems.

To calculate Henry's law constant for each molecule type, only the two lowest reduced pressures were used. Ethyl butyrate molecules do not exhibit ideal loading behavior at 2 and 4% reduced pressures; thus, simulations at 0.5 and 1% reduced pressures were carried out to observe ideal loading behavior. Henry's law constants for each solute are presented in Table 3. The large value for ethyl butyrate is likely due to an overestimation of the ethyl butyrate−surfactant interactions in the SDK force field.

For *n*-nonane and 1-hexanol, the transfer free energies are nearly constant with a small decrease (more favorable) for *n*-nonane at high pressures. This behavior is consistent with small positive deviations from Henry's law behavior. In contrast, the transfer free energy of ethyl butyrate increases (becomes less favorable) as a function of pressure, which is consistent with large negative deviations from Henry's law behavior. Both *n*-nonane and 1-hexanol show small positive deviations from ideal loading at high reduced pressures, resulting from additive−additive interactions being more favorable than additive−surfactant interactions. The somewhat smaller positive deviation from Henry's law behavior and the nearly constant free energy of transfer observed for 1-hexanol than *n*-nonane certainly reflects the stronger interactions of 1-hexanol with the polar groups of the surfactant, but it may also be accentuated by the underprediction of the hexanol−hexanol interactions (as evidenced by the greatly overpredicted vapor pressure). Ethyl butyrate shows a negative deviation from ideal loading due to less favorable additive−additive interactions and too favorable additive−surfactant interactions. Because both 1-hexanol and ethyl butyrate have a hydrophilic bead, one might expect that they would exhibit more similarity in regard to deviation from ideal loading behavior, as can be seen in a hybrid grand canonical Monte Carlo dissipative particle dynamics (DPD) approach where certain alcohols exhibit negative deviation from ideality.[34] The difference in deviation of 1-hexanol and ethyl butyrate molecules from Henry's law behavior is likely due to problems with the SDK force field that underpredicts the strength of 1-hexanol interactions (as indicated by the overestimation of its vapor pressure) and overpredicts the strength of ethyl butyrate−surfactant interactions (as indicated by its very large Henry's law constant) due to the well depths of the EST1−EO and EST1−OA interactions being about 40% larger than the values obtained from the geometric mean rule (but the EST1−CT and EST1−CM well depths are close to the values obtained from the geometric mean rule).

Table 3. Henry's Law Constants, Which Describe Ideal Loading Behavior, for Each Solute in this Study

solute	K_{H} (eq 1)
n-nonane	0.23_4
1-hexanol	1.4_1
ethyl butyrate	14_1

Transverse Position and Orientational Distribution of Solutes. Knowledge of the spatial and orientational distributions of the solute molecules adsorbed in the surfactant bilayer is important for understanding their effects on bilayer structure and stability. For reference, a snapshot of the lamellar phase and symmetrized bead density profiles for water and the surfactant bilayer without adsorbed solute molecules are shown in Figure 3. The highest density of the hydrophobic tail, CT, beads is found at the center of the bilayer ($d_\perp$ = 0 Å). The maximum for the hydrophilic head, OA, beads is found at $d_\perp \approx$ 15 Å, and the water density at this location is ≈0.6 g/cm^3. The average position of the water/monolayer interface, determined here as the midpoint between the distances at which the density of the water is 10 and 90% of the density of neat water, is found at $d_\perp \approx$ 14 Å. Water reaches its bulk density at $d_\perp \approx$ 24 Å. We define the bilayer's thickness to be the distance between the two water/monolayer interfaces, i.e., about 28 Å for the bilayer void of solute molecules. Small-angle neutron scattering experiments of a C10E3/water lamellar system at comparable conditions yielded a bilayer thickness of 27.6 Å,

DOI: 10.1021/acs.langmuir.8b00687
Langmuir 2018, 34, 8245−8254

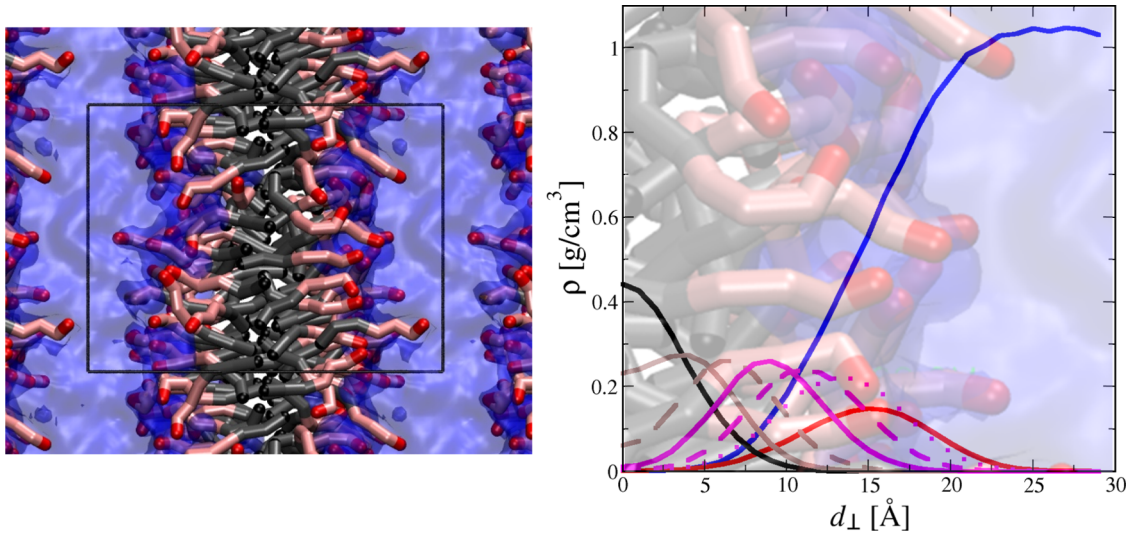

Figure 3. Snapshot of an equilibrated C10E3 surfactant bilayer, void of solute molecules (left). Water is shown as a blue transparent surface. CT, CM, EO, and OA beads are shown in black, gray, pink, and red, respectively. The simulation box, shown as a thin black line, is replicated in all directions to show periodicity. Symmetrized density profile of the equilibrated C10E3 surfactant bilayer (right). The *x*-axis shows the distance perpendicular to the center of the bilayer ($d_\perp$ = 0 Å). The colors denote different bead types: CT (black), CM (brown), EO (magenta), and OA (red) beads of the C10E3 surfactants and W (blue) bead for water. The solid, dashed, and dotted lines denote the first, second, and third instances, respectively, of a CM or EO bead counting from the CT tail.

based on the change of interlayer spacing as the C10E3 volume fraction is varied.[18]

The position of the solute molecules loading into the bilayer at different reduced pressures is illustrated in symmetrized density profiles (see Figure 4) and snapshots (see Figure 5). The nonpolar *n*-nonane molecules have a strong preference to load into the center of the bilayer, as indicated by the density maximum found at $d_\perp$ = 0 Å and by the density decaying to 50% at $d_\perp \approx$ 5 Å. Conversely, the polar 1-hexanol and ethyl butyrate molecules load close to the OA beads of C10E3 and water. At intermediate reduced pressure of the solute molecules, the highest density of the hydrophilic bead of both 1-hexanol and ethyl butyrate is found at $d_\perp \approx$ 8 Å, i.e., close to the EO beads of C10E3. At high reduced pressure, the polar 1-hexanol and ethyl butyrate molecules are fairly evenly distributed throughout the bilayer with the maximum density of 1-hexanol and ethyl butyrate being at $d_\perp$ values of 0 and 8 Å, respectively. Somewhat surprisingly, when adjusting for differences in the bead masses, no significant differences in the density profiles of the nonpolar (CT2 and CM) and the polar (OA and EST1) beads are observed neither for 1-hexanol nor ethyl butyrate, i.e., there is no preference for their hydrophobic parts to be located more toward the center of the bilayer.

Increasing loading of *n*-nonane leads to an increase of the bilayer thickness, or transverse swelling in the *z*-direction (as indicated by the EO and water density profiles shifting to larger $d_\perp$ values), due to formation of a region with high *n*-nonane concentration in the center between the bilayer leaflets and partial displacement of the surfactants (top row of Figure 5). This is in agreement with DPD simulations of a lamellar C12E6 system containing *n*-octadecane solutes, where the repeat distance of the lamellar phase was found to increase at higher solute concentrations, decreasing the concentration of surfactant at the center of the bilayer.[31] Figure 5 also shows the bilayer expanding laterally, in the *x*,*y*-plane, from increased numbers of 1-hexanol or ethyl butyrate molecules loading in between individual surfactants. At a reduced pressure of 32%

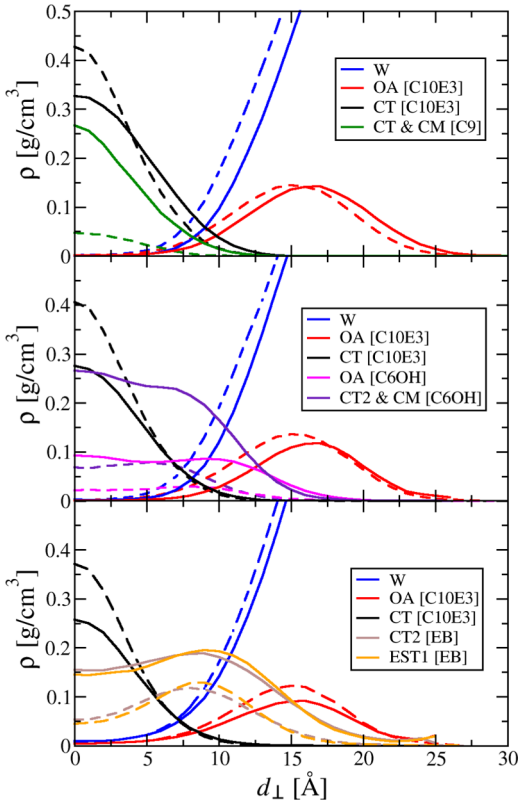

Figure 4. Symmetrized density profiles of the equilibrated C10E3 surfactant bilayer systems after loading of *n*-nonane (top), 1-hexanol (middle), and ethyl butyrate (bottom). The dashed and solid lines denote the 16 and 64% p_{sat} systems for *n*-nonane and 1-hexanol, respectively (8 and 32% p_{sat} for ethyl butyrate). Bead types are identified by different colors as denoted in the legends.

p_{sat}, the loading of ethyl butyrate molecules overwhelms the bilayer (the ethyl butyrate to C10E3 mole ratio is 2:1, see

DOI: 10.1021/acs.langmuir.8b00687
Langmuir 2018, 34, 8245−8254

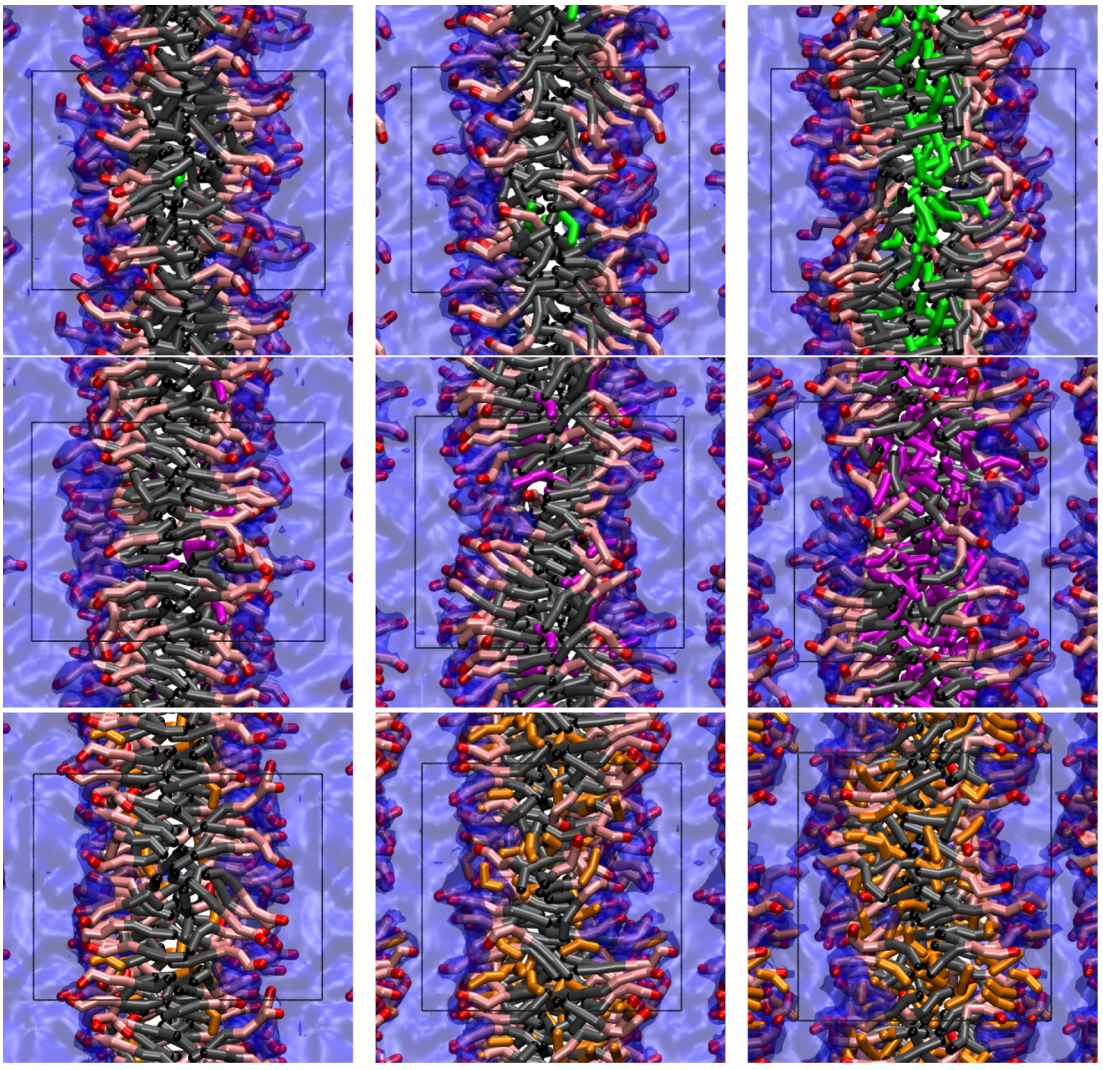

Figure 5. Snapshots of C10E3/W mesophases after loading with *n*-nonane (top), 1-hexanol (middle), and ethyl butyrate (bottom). The left, middle, and right snapshots are for the 4, 16, and 64% p_{sat} systems for *n*-nonane and 1-hexanol, respectively (2, 8, and 32% p_{sat} for ethyl butyrate). Colors as in Figure 2, with the addition of green, magenta, and orange for *n*-nonane, 1-hexanol, and ethyl butyrate, respectively. The simulation box, shown as a thin black line, is replicated in all directions to show periodicity, and all snapshots use the same scale.

Figure 1) and the water region no longer reaches bulk density (see Figure S3).

The orientation at a given position of the solutes loading into the bilayer at different reduced pressures is analyzed via plotting the orientational order parameter versus distance (see Figure 6). The S_{CD} order parameter is a measure of the anisotropy of a particular C−D, carbon−deuterium, bond that yields its time-averaged (ensemble-averaged) orientation.[54−57] For the coarse-grained SDK models, the orientation of C−D bonds cannot be deduced, but an analogous order parameter (S) can be computed according to eq 4[54−57]

$$S = 0.5\langle 3\cos^2\theta - 1\rangle \quad (4)$$

where θ is the angle formed between the z-axis vector and the vector formed between beads separated by two bonds (note that all three solute molecules consist of three SDK beads). When molecules load with a perpendicular, parallel, or random orientation to the bilayer surface, the value of S is equal to 1, −0.5, or 0, respectively. In addition, an S value of 0 can also be observed when all molecules are oriented at an angle of ∼54.7°, known as "the magic angle". Figure 6 shows the localized orientational order parameter (where the z-position of the solute's central bead is used to specify the location).

The *n*-nonane molecules exhibit no preference for any orientation (with respect to the interface) near the center of the bilayer at all reduced pressures. At 4 Å < $d_\perp$ < 8 Å, the *n*-nonane molecules show a slight preference for a perpendicular orientation (i.e., aligned with the surfactant molecules). For 1-hexanol, the molecules are randomly oriented near the central part of the bilayer between the two leaflets ($d_\perp$ < 2 Å), but a pronounced preference for perpendicular orientations emerges at larger $d_\perp$ values, and this preference is strongest near the surfactant−water interface ($d_\perp \approx$ 15 Å). Similarly to *n*-nonane, ethyl butyrate molecules exhibit no preference for any orientation at $d_\perp$ < 4 Å. Near the polar region of the surfactant molecules, ethyl butyrate shows a preference for a perpendicular orientation that is similarly pronounced as for *n*-nonane, but much weaker than that for 1-hexanol. Overall, all three solute types show a preference for orientations perpendicular to the interface near the EO−OA section of the C10E3 surfactants, which indicates that alignment with the C10E3 is entropically favored, but the stronger alignment of 1-

DOI: 10.1021/acs.langmuir.8b00687
Langmuir 2018, 34, 8245−8254

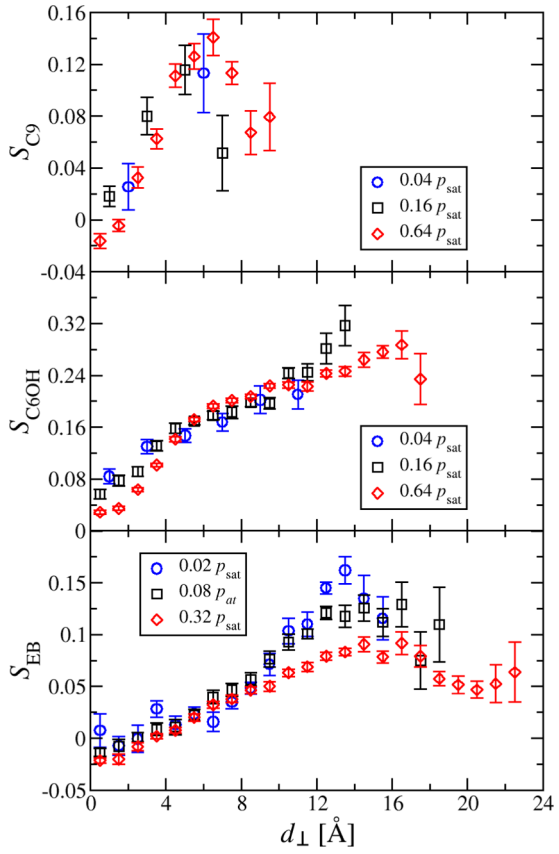

Figure 6. Orientational order parameters for *n*-nonane (top), 1-hexanol (middle), and ethyl butyrate (bottom) molecules as a function of their distance from the center of the equilibrated C10E3 surfactant bilayer. The bin sizes are selected to reflect the solute loading of the different systems: 4 Å for *n*-nonane at 0.04 p_{sat}, 2 Å for *n*-nonane at 0.16 p_{sat} and 1-hexanol at 0.04 p_{sat}, and 1 Å for all other systems. If the number of solutes observed at a certain $d_\perp$ value across all 1200 configurations analyzed is less than 400, then that data point is omitted. Different pressures are identified by different colors and symbols as denoted in the legends.

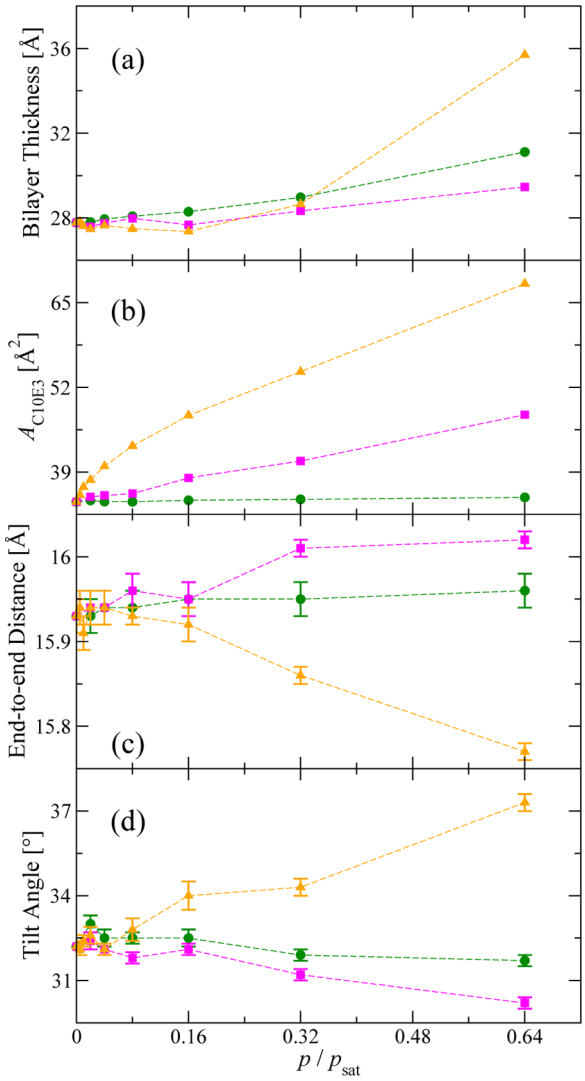

Figure 7. Bilayer thickness (a), head-group area per surfactant molecule (b), end-to-end distance of surfactant molecules (c), and tilt angle of surfactant molecules with respect to the bilayer normal (d) versus the reduced saturated vapor pressure of solute. The green circles, magenta squares, and orange triangles represent *n*-nonane, 1-hexanol, and ethyl butyrate, respectively. The dashed lines are drawn for clarity.

hexanol indicates a contribution from its polar group preferring orientations that allow for interactions with interfacial water.

Structural Analysis of Surfactant Bilayer. The effects of solute uptake on the bilayer structure are illustrated by changes in the bilayer thickness, surfactant head-group area, end-to-end distance, and tilt angle (see Figure 7), as well as surfactant orientational order parameter (see Figure 8). The bilayer thickness is taken as the distance between the two water/monolayer interfaces; the surfactant head-group area is calculated as the total cross-sectional area of the two interfaces in the *x*,*y*-plane (these have equal area in the orthogonal simulation box) divided by the number of surfactant molecules (note that the number of C10E3 molecules in each leaflet is balanced with the exception of ethyl butyrate at 64% p_{sat}); the end-to-end vector from the OA to the CT bead is used to calculate the surfactant length; the surfactant tilt angle is the angle formed between the end-to-end vector and a vector normal to the *x*,*y*-plane. Because the loading of the nonpolar *n*-nonane molecules is relatively low (see Figure 1), the structure of the bilayer is least affected. At p = 64% p_{sat}, the bilayer thickness is increased by about 3 Å (10%), but there is no lateral expansion of the bilayer (measured by the area per surfactant molecule) because the nonpolar *n*-nonane molecules do not populate the region between the EO_3−OA headgroup of the surfactants. The population of *n*-nonane in the tail region of the surfactants leads to a very slight increase of the end-to-end distance and reduction of the tilt angle. In contrast, uptake of 1-hexanol and ethyl butyrate molecules leads to a lateral expansion of the bilayer by about 11 Å^2 per additive molecule (note that the number of ethyl butyrate molecules exceeds that of 1-hexanol by almost a factor of three at higher reduced pressures). This increase in lateral area is less than the cross section of these additive molecules and much smaller than the area per surfactant molecule of 35 Å^2 for the additive-free bilayer because these additive molecules also load in the hydrophobic core of the bilayer and lead to an increase in the bilayer thickness. Because the surfactant to water ratio is fixed, the lateral expansion of the bilayer leads to a thinning of the water region (see also Figure 5). A difference in the effect of 1-hexanol and ethyl butyrate molecules on the bilayer can be seen in the surfactant tilt angle and end-to-end distance. 1-

DOI: 10.1021/acs.langmuir.8b00687
Langmuir 2018, 34, 8245−8254

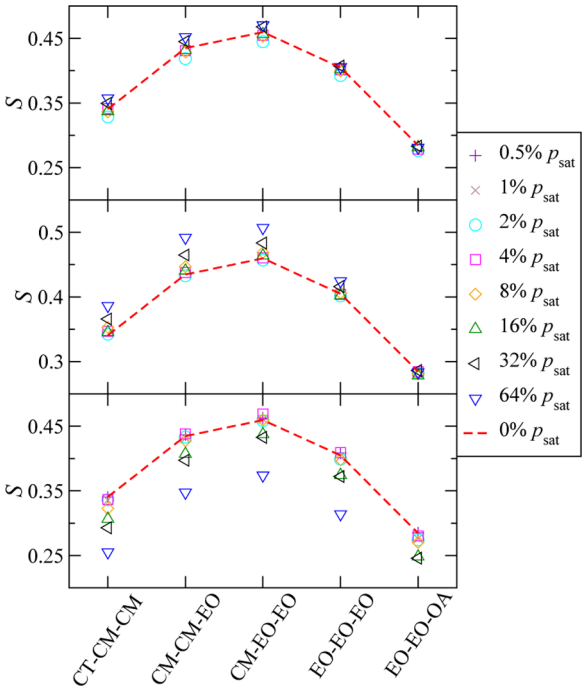

Figure 8. Orientational order parameter versus 1−3 bead vector of surfactant in the *n*-nonane (top), 1-hexanol (middle), and ethyl butyrate (bottom) systems. Colors are shown in the legend.

Hexanol molecules cause an increase in surfactant end-to-end distance along with a decrease in tilt angle as reduced pressure increases. In contrast, ethyl butyrate molecules decrease the surfactant end-to-end distance and increase the tilt angle as the reduced pressure is increased.

Figure 8 displays the orientational order parameter along the backbone of the C10E3 molecules with respect to the water/monolayer interface. The general shape of the curves describing the order parameter of the C10E3 molecules is similar for all systems. The CM−CM−EO and CM−EO−EO vectors contain nonpolar and polar beads, and the amphiphilic nature leads to a preference for the CM bead to be in the hydrophobic region and the EO bead to be in the hydrophilic region of the bilayer; thus, the CM−CM−EO and CM−EO−EO vectors exhibit a higher degree of perpendicular alignment compared to the other vectors in the surfactants. Comparing both ends, we find that the EO−EO−OA vector consisting only of hydrophilic beads exhibits the least preference for alignment perpendicular to the interface presumably because of the encroachment of water molecules, whereas the CT−CM−CM vector consisting of all hydrophobic beads shows intermediate alignment presumably because the tails of surfactants in opposing leaflets can interdigitate.

Comparing the effect of additive loading on surfactant order parameter gives insight into how the solutes affect the individual surfactant molecules. Because loading of *n*-nonane molecules is relatively low, and these load mainly at the center of the bilayer between its leaflets, an increase in *n*-nonane reduced pressure has only a small effect on the order parameter of the surfactants, namely, a small shift toward higher *S* values for the hydrophobic part of C10E3 due to interdigitation of *n*-nonane molecules. As the loading of 1-hexanol molecules increases with increasing reduced pressure, the largest shift in order parameter is found near the middle of the surfactant chain. 1-Hexanol molecules, unlike *n*-nonane and similar to ethyl butyrate, load near the middle region of the surfactant layer itself (see Figure 4). Increasing the loading of 1-hexanol is found to increase the orientational order of the surfactants. In contrast, the loading of ethyl butyrate molecules leads to a decrease in the *S* values for all 1−3 vectors of the surfactant. This suggests that the ethyl butyrate molecules disturb the full span of the bilayer (see Figure 4).

On the basis of the structural analysis presented here, it is likely that lamellar C10E3 mesophase of the *n*-nonane loaded system at 64% p_{sat} is thermodynamically stable in agreement with experimental studies of a ternary C10E3/water/*n*-dodecane system that exhibits stability at similar compositions (1:1:0.1 by weight at 64% p_{sat}) and temperatures due to being in the liquid crystalline phase.[14] For the SDK model, the system loaded with ethyl butyrate (1:1:1.2 by weight at 64% p_{sat}) is likely only marginally stable as a lamellar phase, but the system size investigated here (and free-energy barriers for structural transitions) may hinder the transformation to reverse micelles.

CONCLUSIONS

Monte Carlo simulations in the osmotic Gibbs ensemble have been conducted to study the loading behavior of *n*-nonane, 1-hexanol, and ethyl butyrate into a C10E3/water−surfactant bilayer and the resulting structural changes. Both *n*-nonane and 1-hexanol molecules are observed to exhibit positive deviations from Henry's law behavior at high reduced pressures (above 32% p_{sat}). Ethyl butyrate molecules, on the other hand, exhibit a negative deviation from ideal loading behavior already at intermediate reduced pressures (above 4% p_{sat}). It should be noted that the ethyl butyrate−surfactant interactions appear to be overestimated, and using EST1−OA and EST1−EO well depths closer to the geometric mean rule would lead to a less favorable free energy of transfer and lower loading of ethyl butyrate molecules. More favorable hexanol−hexanol interactions (as surmised by the large overestimation of its vapor pressure) would not affect 1-hexanol loading at low reduced pressure, but lead to somewhat larger positive deviations from Henry's law behavior at higher reduced pressures. The simulations show that *n*-nonane molecules cause an increase of the bilayer thickness without any lateral expansion (as measured by the area per surfactant molecule), whereas loading of both 1-hexanol and ethyl butyrate molecules causes predominantly a lateral expansion, but also a relatively smaller increase in bilayer thickness. Combining our observations from symmetrized density profiles and orientational distributions of the solutes, we conclude that *n*-nonane molecules load in the center of the surfactant bilayer without orientational preference at all reduced pressures. In contrast, both 1-hexanol and ethyl butyrate molecules load near the EO beads of the surfactants, with a preference for perpendicular orientations (more pronounced for 1-hexanol) with respect to the water/monolayer interface. At their highest reduced pressures, both polar solutes are evenly distributed throughout their respective bilayers. Surfactant end-to-end distance, tilt angle, and order parameter analysis provide evidence that loading with both *n*-nonane and 1-hexanol molecules slightly increases the surfactant's orientational order, whereas ethyl butyrate has the opposite effect. The simulation technique used herein can also be used to study not just lamellar phases, but also micellar aggregates and to more detailed molecular models (e.g., united-atom models for surfactant and multisite models for each individual water molecule) or to coarse-grained models

DOI: 10.1021/acs.langmuir.8b00687
Langmuir 2018, 34, 8245−8254

for more complex amphiphilic molecules, e.g., block copolymers, as is the subject for future study.

■ ASSOCIATED CONTENT

Supporting Information

The Supporting Information is available free of charge on the ACS Publications website at DOI: 10.1021/acs.langmuir.8b00687.

Parameters for non-bonded interactions (Table S1); harmonic bond stretching parameters (Table S2); harmonic angle bending parameters (Table S3); numerical data for Figures 1, 3, 4, 7, and 8 (Tables S4 − S9); additive loading versus Monte Carlo cycles (Figure S1); mole fractions of additives versus reduced pressure (Figure S2); version of Figure 4 with full density range (Figure S3); snapshots of bilayer systems at additional values of the reduced pressure (Figure S4) (PDF)

■ AUTHOR INFORMATION

Corresponding Author

*E-mail: siepmann@umn.edu.

ORCID

Mona S. Minkara: 0000-0003-1821-2725

Rebecca K. Lindsey: 0000-0002-3438-9064

Peter H. Koenig: 0000-0002-6512-5686

J. Ilja Siepmann: 0000-0003-2534-4507

Notes

The authors declare no competing financial interest.

■ ACKNOWLEDGMENTS

This research was supported by the National Science Foundation (CBET-1159837), the Procter & Gamble Company, a National Academy of Sciences Ford Foundation Fellowship awarded to M.S.M., and the University of Minnesota Disability Resource Center through access assistants for Dr. Minkara, specifically to John Hamill, Tyler Westland, and Tanner Lambson. Computer resources were provided by the Minnesota Supercomputing Institute. We thank the members of the Siepmann group at the University of Minnesota for constructive comments, particularly Tyler Josephson.

■ REFERENCES

(1) Stephenson, B. C.; Rangel-Yagui, C. O.; Pessoa, A.; Tavares, L. C.; Beers, K.; Blankschtein, D. Experimental and Theoretical Investigation of the Micellar-Assisted Solubilization of Ibuprofen in Aqueous Media. *Langmuir* **2006**, *22*, 1514−1525.

(2) Narang, A. S.; Delmarre, D.; Gao, D. Stable Drug Encapsulation in Micelles and Microemulsions. *Int. J. Pharm.* **2007**, *345*, 9−25.

(3) Williams, H. D.; Trevaskis, N. L.; Charman, S. A.; Shanker, R. M.; Charman, W. N.; Pouton, C. W.; Porter, C. J. H. Strategies to Address Low Drug Solubility in Discovery and Development. *Pharmacol. Rev.* **2013**, *65*, 315−499.

(4) Gosangari, S.; Dyakonov, T. Enhanced Dissolution Performance of Curcumin with the Use of Supersaturatable Formulations. *Pharm. Dev. Technol.* **2013**, *18*, 475−480.

(5) Schulz, R.; Yamamoto, K.; Klossek, A.; Flesch, R.; Hönzke, S.; Rancan, F.; Vogt, A.; Blume-Peytavi, U.; Hedtrich, S.; Schäfer-Korting, M.; Rühl, E.; Netz, R. R. Data-Based Modeling of Drug Penetration Relates Human Skin Barrier Function to the Interplay of Diffusivity and Free-Energy Profiles. *Proc. Natl. Acad. Sci. U.S.A.* **2017**, *114*, 3631−3636.

(6) Bu, G.; Yang, Y.; Chen, F.; Liao, Z.; Gao, Y.; Yang, H.; Li, R.; Liu, K.; Zhao, J. Extraction and Physicochemical Properties of Soya Bean Protein and Oil by a New Reverse Micelle System Compared with Other Extraction Methods. *Int. J. Food Sci. Technol.* **2014**, *49*, 1079−1089.

(7) Somasundaran, P.; Chakraborty, S.; Qiang, Q.; Deo, P.; Wang, J.; Zhang, R. Surfactants, Polymers, and Their Nanoparticles for Personal Care Applications. *J. Cosmet. Sci.* **2004**, *55*, S1−S17.

(8) Lukowicz, T.; Company Maldonado, R.; Molinier, V.; Aubry, J. M.; Nardello-Rataj, V. Fragrance Solubilization in Temperature Insensitive Aqueous Microemulsions Based on Synergistic Mixtures of Nonionic and Anionic Surfactants. *Colloids Surf., A* **2014**, *458*, 85−95.

(9) Cui, Z.; Ding, J.; Scoles, L.; Wang, Q.; Chen, Q. Superhydrophobic Surfaces Fabricated by Spray-Coating Micelle Solutions of Comb Copolymers. *Colloid Polym. Sci.* **2013**, *291*, 1409−1418.

(10) Rane, S. S.; Anderson, B. D. What Determines Drug Solubility in Lipid Vehicles: Is It Predictable? *Adv. Drug Delivery Rev.* **2008**, *60*, 638−656.

(11) Lawrence, M. J. Surfactant Systems: Their Use in Drug Delivery. *Chem. Soc. Rev.* **1994**, *23*, 417−424.

(12) Li, P.; Ghosh, A.; Wagner, R. F.; Krill, S.; Joshi, Y. M.; Serajuddin, A. T. M. Effect of Combined Use of Nonionic Surfactant on Formation of Oil-In-Water Microemulsions. *Int. J. Pharm.* **2005**, *288*, 27−34.

(13) Kawakami, K.; Oda, N.; Miyoshi, K.; Funaki, T.; Ida, Y. Solubilization Behavior of a Poorly Soluble Drug Under Combined Use of Surfactants and Cosolvents. *Eur. J. Pharm. Sci.* **2006**, *28*, 7−14.

(14) Ali, A. A.; Mulley, B. A. Formation of Liquid Crystal and Other Non-Fluid Phases in Emulsions Containing Non-Ionic Surfactants. *J. Pharm. Pharmacol.* **1978**, *30*, 205−213.

(15) Mitchell, D. J.; Tiddy, G. J. T.; Waring, L.; Bostock, T.; McDonald, M. P. Phase Behaviour of Polyoxyethylene Surfactants with Water. *J. Chem. Soc., Faraday Trans. 1* **1983**, *79*, 975−1000.

(16) Cao, Y.; Marra, M.; Anderson, B. D. Predictive Relationships for the Effects of Triglyceride Ester Concentration and Water Uptake on Solubility and Partitioning of Small Molecules Into Lipid Vehicles. *J. Pharm. Sci.* **2004**, *93*, 2768−2779.

(17) Nagarajan, R. Solubilization by Amphiphilar Aggregates. *Curr. Opin. Colloid Interface Sci.* **1997**, *2*, 282−293.

(18) Le, T. D.; Olsson, U.; Mortensen, K.; Zipfel, J.; Richtering, W. Nonionic Amphiphilic Bilayer Structures Under Shear. *Langmuir* **2001**, *17*, 999−1008.

(19) Ferreira, T. M.; Medronho, B.; Martin, R. W.; Topgaard, D. Segmental Order Parameters in a Nonionic Surfactant Lamellar Phase Studied with ^{1}H-^{13}C Solid-State NMR. *Phys. Chem. Chem. Phys.* **2008**, *10*, 6033−6038.

(20) Schönhoff, M.; Söderman, O.; Li, Z. X.; Thomas, R. K. Internal Dynamics and Order Parameters in Surfactant Aggregates: A 2H NMR Study of Adsorption Layers and Bulk Phases. *Langmuir* **2000**, *16*, 3971−3976.

(21) Ward, A. J. I.; Ku, H.; Phillippi, M. A.; Marie, C. Order of Polyoxyethylene Chains in the Lamellar Phase of a Nonionic Surfactant. *Mol. Cryst. Liq. Cryst. Incorporating Nonlinear Opt.* **1988**, *154*, 55−60.

(22) Tyrode, E.; Johnson, C. M.; Kumpulainen, A.; Rutland, M. W.; Claesson, P. M. Hydration State of Nonionic Surfactant Monolayers at the Liquid/Vapor Interface: Structure Determination by Vibrational Sum Frequency Spectroscopy. *J. Am. Chem. Soc.* **2005**, *127*, 16848−16859.

(23) Nibu, Y.; Inoue, T. Phase Behavior of Aqueous Mixtures of Some Polyethylene Glycol Decyl Ethers Revealed by DSC and FT-IR Measurements. *J. Colloid Interface Sci.* **1998**, *205*, 305−315.

(24) Sottmann, T.; Strey, R.; Chen, S.-H. A Small-Angle Neutron Scattering Study of Nonionic Surfactant Molecules at the Water-Oil Interface: Area Per Molecule, Microemulsion Domain Size, and Rigidity. *J. Chem. Phys.* **1997**, *106*, 6483−6491.

(25) Nilsson, P. G.; Lindman, B. Water Self-Diffusion in Nonionic Surfactant Solutions. Hydration and Obstruction Effects. *J. Phys. Chem.* **1983**, *87*, 4756−4761.
(26) Klose, G.; Eisenblätter, S.; Galle, J.; Islamov, A.; Dietrich, U. Hydration and Structural Properties of a Homologous Series of Nonionic Alkyl Oligo (Ethylene Oxide) Surfactants. *Langmuir* **1995**, *11*, 2889−2892.
(27) Goldstein, R. E. On the Theory of Lower Critical Solution Points in Hydrogen-Bonded Mixtures. *J. Chem. Phys.* **1984**, *80*, 5340−5341.
(28) Karaborni, S.; van Os, N. M.; Esselink, K.; Hilbers, P. A. J. Molecular Dynamics Simulations of Oil Solubilization in Surfactant Solutions. *Langmuir* **1993**, *9*, 1175−1178.
(29) Larson, R. G. Monte Carlo Simulation of Microstructural Transitions in Surfactant Systems. *J. Chem. Phys.* **1992**, *96*, 7904−7918.
(30) Woodhead, J. L.; Hall, C. K. Simulation of Micelle Formation in the Presence of Solutes. *Langmuir* **2010**, *26*, 15135−15141.
(31) Denham, N.; Holmes, M. C.; Zvelindovsky, A. V. The Phases in a Non-ionic Surfactant ($C_{12}E_6$)-Water Ternary System: A Coarse-Grained Computer Simulation. *J. Phys. Chem. B* **2011**, *115*, 1385−1393.
(32) Rane, S. S.; Anderson, B. D. Molecular Dynamics Simulations of Functional Group Effects on Solvation Thermodynamics of Model Solutes in Decane and Tricaprylin. *Mol. Pharmaceutics* **2008**, *5*, 1023−1036.
(33) Sanders, S. A.; Sammalkorpi, M.; Panagiotopoulos, A. Z. Atomistic Simulations of Micellization of Sodium Hexyl, Heptyl, Octyl, and Nonyl Sulfates. *J. Phys. Chem. B* **2012**, *116*, 2430−2437.
(34) Rodgers, J. M.; Webb, M.; Smit, B. Alcohol Solubility in a Lipid Bilayer: Efficient Grand-Canonical Simulation of an Interfacially Active Molecule. *J. Chem. Phys.* **2010**, *132*, No. 064107.
(35) Floriano, M. A.; Caponetti, E.; Panagiotopoulos, A. Z. Micellization in Model Surfactant Systems. *Langmuir* **1999**, *15*, 3143−3151.
(36) Siepmann, J. I.; Karaborni, S.; Klein, M. L. Monte-Carlo Simulation of the Liquid-Vapor Coexistence in a Langmuir Monolayer of Pentadecanoic Acid. *J. Phys. Chem.* **1994**, *98*, 6675−6678.
(37) Klamt, A.; Huniar, U.; Spycher, S.; Keldenich, J. COSMOmic: A Mechanistic Approach to the Calculation of Membrane-Water Partition Coefficients and Internal Distributions within Membranes and Micelles. *J. Phys. Chem. B* **2008**, 12148−12157.
(38) Rekvig, L.; Frenkel, D. Molecular Simulations of Droplet Coalescence in Oil/Water/Surfactant Systems. *J. Chem. Phys.* **2007**, *127*, No. 134701.
(39) Panagiotopoulos, A. Z.; Quirke, N.; Stapleton, M.; Tildesley, D. J. Phase Equilibria by Simulation in the Gibbs Ensemble. *Mol. Phys.* **1988**, *63*, 527−545.
(40) Shinoda, W.; Devane, R.; Klein, M. L. Multi-Property Fitting and Parameterization of a Coarse Grained Model for Aqueous Surfactants. *Mol. Simul.* **2007**, *33*, 27−36.
(41) Shinoda, W.; DeVane, R.; Klein, M. L. Coarse-Grained Molecular Modeling of Non-Ionic Surfactant Self-Assembly. *Soft Matter* **2008**, *4*, 2454−2462.
(42) Panagiotopoulos, A. Z. Direct Determination of Phase Coexistence Properties of Fluids by Monte Carlo Simulation in a New Ensemble. *Mol. Phys.* **2002**, *100*, 237−246.
(43) Martínez, L.; Andrade, R.; Birgin, E. G.; Martinez, J. M. PACKMOL: A Package for Building Initial Configurations for Molecular Dynamics Simulations. *J. Comput. Chem.* **2009**, *30*, 2157−2164.
(44) Parrinello, M.; Rahman, A. Polymorphic Transitions in Single Crystals: A New Molecular Dynamics Method. *J. Appl. Phys.* **1981**, *52*, 7182−7190.
(45) Yashonath, S.; Rao, C. N. R. A Monte Carlo Study of Crystal Structure Transformations. *Mol. Phys.* **1985**, *54*, 245−251.
(46) Siepmann, J. I.; Martin, M. G.; Chen, B.; Wick, C. D.; Stubbs, J. M.; Potoff, J. J.; Eggimann, B. L.; McGrath, M. J.; Zhao, X. S.; Anderson, K. E.; Rafferty, J. L.; Rai, N.; Maerzke, K. A.; Keasler, S. J.; Bai, P.; Fetisov, E. O.; Shah, M. S.; Chen, Q. P.; DeJaco, R. F.; Chen, J. L.; Bai, X. *Monte Carlo for Complex Chemical Systems—Minnesota*, version 17.1; University of Minnesota: Minneapolis, MN, 2017.
(47) Shinoda, W.; Devane, R.; Klein, M. L. Zwitterionic Lipid Assemblies: Molecular Dynamics Studies of Monolayers, Bilayers, and Vesicles Using a New Coarse Grain Force Field. *J. Phys. Chem. B* **2010**, *114*, 6836−6849.
(48) Siepmann, J. I.; Frenkel, D. Configurational Bias Monte Carlo: A New Sampling Scheme for Flexible Chains. *Mol. Phys.* **1992**, *75*, 59−70.
(49) Vlugt, T. J. H.; Martin, M. G.; Smit, B.; Siepmann, J. I.; Krishna, R. Improving the Efficiency of the Configurational-Bias Monte Carlo Algorithm. *Mol. Phys.* **1998**, *94*, 727−733.
(50) Mooij, G. C. A. M.; Frenkel, D.; Smit, B. Direct Simulation of Phase Equilibria of Chain Molecules. *J. Phys.: Condens. Matter* **1992**, *4*, L255−L259.
(51) Carruth, G. F.; Kobayashi, R. Vapor Pressure of Normal Paraffins Ethane Through *n*-Decane from Their Triple Points to About 10 Mm Hg. *J. Chem. Eng. Data* **1973**, *18*, 115−126.
(52) Nasirzadeh, K.; Neueder, R.; Kunz, W. Vapor Pressure Determination of the Aliphatic C_5 to C_8 1-Alcohols. *J. Chem. Eng. Data* **2006**, *51*, 7−10.
(53) Stull, D. R. Vapor Pressure of Pure Substances: Organic Compounds. *Ind. Eng. Chem.* **1947**, *39*, 517−540.
(54) Schindler, H.; Seelig, J. Deuterium Order Parameters in Relation to Thermodynamic Properties of a Phospholipid Bilayer. A Statistical Mechanical Interpretation. *Biochemistry* **1975**, *14*, 2283−2287.
(55) Berger, O.; Edholm, O.; Jähnig, F. Molecular Dynamics Simulations of a Fluid Bilayer of Dipalmitoylphosphatidylcholine at Full Hydration, Constant Pressure, and Constant Temperature. *Biophys. J.* **1997**, *72*, 2002−2013.
(56) Marčelja, S. Chain Ordering in Liquid Crystals. I. Even-Odd Effect. *J. Chem. Phys.* **1974**, *60*, 3599−3604.
(57) Marčelja, S. Chain Ordering in Liquid Crystals. II. Structure of Bilayer Membranes. *Biochim. Biophys. Acta, Biomembr.* **1974**, *367*, 165−176.

DOI: 10.1021/acs.langmuir.8b00687
Langmuir 2018, 34, 8245−8254